

# Majorana Zero Modes Protected by Hopf Invariant in Topologically Trivial Superconductors

Zhongbo Yan,<sup>1</sup> Ren Bi,<sup>1</sup> and Zhong Wang<sup>1,2,\*</sup>

<sup>1</sup>*Institute for Advanced Study, Tsinghua University, Beijing, 100084, China*

<sup>2</sup>*Collaborative Innovation Center of Quantum Matter, Beijing, 100871, China*

Majorana zero modes are usually attributed to topological superconductors. We study a class of two-dimensional topologically trivial superconductors without chiral edge modes, which nevertheless host robust Majorana zero modes in topological defects. The construction of the specific single-band model is facilitated by the Hopf map and the Hopf invariant. This work will stimulate investigations of Majorana zero modes in superconductors in the topologically trivial regime.

PACS numbers: 73.43.-f, 71.70.Ej, 74.25.-q

Majorana zero modes (or Majorana bound states) are exotic excitations predicted to exist in the vortex cores[1, 2] of two-dimensional (2D) topological superconductors[3–7] and at the ends of 1D topological superconductors[8]. Spatially separated Majorana zero modes give rise to degenerate ground states, which encode qubits immune to local dechoerence[8, 9]. Furthermore, unitary transformations among the ground states can be implemented by braiding[10–13] or measurements[14, 15] of these modes, indicating that such qubits may become building blocks of topological quantum computers[16–20]. Therefore, Majorana zero modes have been vigorously pursued in condensed matter physics[21–27].

There have been a great variety of proposals for topological superconductors, including 2D semiconductor heterostructures[28, 29], topological-insulator-superconductor proximity[30–34], 1D spin-orbit-coupled quantum wires[35–41], Shockley mechanism[42], and cold atom systems in 2D[43–46] and 1D[47, 48], etc. Experimentally, suggestive signatures of Majorana zero modes in both 1D[49–58] and 2D[59–64] topological superconductors have been found.

It is often implicitly assumed that topological superconductivity is a prerequisite for Majorana zero modes, accordingly, the chiral edge modes go hand in hand with the vortex zero modes in 2D superconductors. In this paper we show that certain topological defects[65–70] in 2D topologically *trivial* superconductors can support robust Majorana zero modes. Somewhat surprisingly, single-band superconductors suffice this purpose. The model Hamiltonian is related to the *Hopf maps*, which originally refer to nontrivial mappings from a 3D sphere  $S^3$  to a 2D sphere  $S^2$ , characterized by the integer Hopf invariant[71]. Mappings from a 3D torus  $T^3$  to  $S^2$  inherit the nontrivial topology from the mappings  $S^3 \rightarrow S^2$ . The Hopf invariant has found interesting applications in nonlinear-sigma models and spin chains[71, 72], Hopf insulators[73–78], and quench dynamics of Chern insulators[79, 80].

Our model describes topologically trivial superconductors with zero Chern number and no chiral edge state. Nevertheless, a topological point-defect is characterized by a Hopf invariant defined in the  $(k_x, k_y, \theta)$  space, where  $k_x, k_y$  are crystal momenta and  $\theta$  is the polar angle[81](Fig.1a). The parity (even/odd) of Hopf invariant determines the presence (ab-

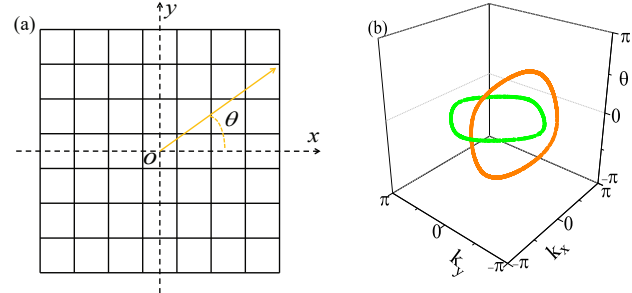


FIG. 1. (a) Sketch. The Hamiltonian varies as a function of  $\theta$ , creating a defect at  $O = (x_0, y_0)$ . ( $r = \sqrt{(x - x_0)^2 + (y - y_0)^2}$ ,  $\theta = \arctan(y - y_0)/(x - x_0)$ ). (b) The inverse images of  $(0, 0, 1)$  (green circle) and  $(1, 0, 0)$  (orange circle) of the mapping  $\hat{\mathbf{d}}(\mathbf{k}, \theta) : T^3 \rightarrow S^2$ .

sence) of robust Majorana zero mode, though the superconductor for every fixed  $\theta$  is topologically trivial. Stimulated by this mechanism, which significantly differs from the magnetic-vortex origin of zero mode in topological  $p$ -wave superconductor[1, 2], we also design trivial-superconductor-based (and vortex-free) T-junctions harboring Majorana zero modes.

*Zero modes.*—Before studying topological defects, we consider spatially uniform 2D single-band Bogoliubov-de Gennes (BdG) Hamiltonians parameterized by  $\lambda$ :

$$H(\mathbf{k}, \lambda) = \begin{pmatrix} \xi_{\mathbf{k}}(\lambda) & \Delta_{\mathbf{k}}(\lambda) \\ \Delta_{\mathbf{k}}^*(\lambda) & -\xi_{-\mathbf{k}}(\lambda) \end{pmatrix} \quad (1)$$

where  $\mathbf{k} = (k_x, k_y)$ ,  $\xi_{\mathbf{k}} = E_{\mathbf{k}} - \mu$ ,  $E_{\mathbf{k}}$  and  $\mu$  is the energy and chemical potential, respectively, and  $\Delta_{\mathbf{k}}$  is the Cooper pairing. It describes single-band spinless (or spin-fully-polarized) superconductors. This Hamiltonian can be written in terms of the Pauli matrices  $\tau_i$  as

$$H(\mathbf{k}, \lambda) = \sum_{i=x,y,z} d_i(\mathbf{k}, \lambda) \tau_i, \quad (2)$$

with  $d_x = \text{Re}\Delta_{\mathbf{k}}$ ,  $d_y = -\text{Im}\Delta_{\mathbf{k}}$ ,  $d_z = \xi_{\mathbf{k}}$  (we have  $\xi_{\mathbf{k}} = \xi_{-\mathbf{k}}$  in our model). For reason to become clear shortly, we take

$$d_i = z^{\dagger} \tau_i z, \quad (3)$$

where  $z = (z_\uparrow, z_\downarrow)^T$  and

$$\begin{aligned} z_\uparrow &= \sin k_x + i \sin k_y, \\ z_\downarrow &= \sin \lambda + i[\cos k_x + \cos k_y + \cos \lambda - m_0], \end{aligned} \quad (4)$$

with  $m_0 = \frac{3}{2}$ . We can see that  $z_\uparrow$  is odd while  $z_\downarrow$  is even in  $\mathbf{k}$ , thus  $d_{x,y}(\mathbf{k}) = -d_{x,y}(-\mathbf{k})$ , which is a key property that enables us to view Eq.(2) as a BdG equation. Given Eq.(4), the pairing  $d_{x,y}$  are of the same order as the hopping  $d_z$ . To describe weakly-pairing superconductors, one may consider

$$H_\eta(\mathbf{k}, \lambda) = \eta(d_x \tau_x + d_y \tau_y) + d_z \tau_z, \quad (5)$$

with a small but nonzero  $\eta$ . Nevertheless, tuning the value of  $\eta$  does not close the energy gap, hence it does not qualitatively change the results. Thus we will simply take  $\eta = 1$  below.

Eq.(4) has been adopted in studying three-dimensional Hopf insulators[73–78], with  $\lambda$  replaced by the third momentum  $k_z$ . Our purpose here is different. We study topological defects in 2D superconductors by taking

$$\lambda = n\theta, \quad (6)$$

where  $\theta$  is the polar angle (Fig.1a), and  $n$  is an integer. The unit vector  $\hat{\mathbf{d}}(\mathbf{k}, \theta) \equiv \mathbf{d}/d$  ( $d \equiv |\mathbf{d}|$ ) maps the 3D torus  $T^3$  ( $k_x, k_y, \theta$  are defined modulo  $2\pi$ ) to the 2D unit sphere  $S^2$ . For nonzero  $n$ , the inverse-image circles of two points on  $S^2$  are linked ( $n = 1$  case is shown in Fig.1b). To quantify such linking, the Hopf invariant can be defined[71, 73]:  $N_h = -\frac{1}{4\pi^2} \int d\theta d^2k \epsilon^{\mu\nu\rho} a_\mu \partial_\nu a_\rho$ , where the integrating range is the Brillouin zone for  $\mathbf{k}$  and  $[0, 2\pi]$  for  $\theta$ ,  $a_\mu = -i\langle \psi(\mathbf{k}, \theta) | \partial_\mu | \psi(\mathbf{k}, \theta) \rangle$ , with  $\mu, \nu, \rho = k_x, k_y, \theta$ , and  $|\psi\rangle$  is the negative-energy eigenfunction of  $H(\mathbf{k}, \theta)$ . Alternatively, we can define  $A_\mu = a_\mu/2\pi$ ,  $j^\mu = \epsilon^{\mu\nu\rho} \partial_\nu A_\rho = (1/8\pi) \epsilon^{\mu\nu\rho} \hat{\mathbf{d}} \cdot (\partial_\nu \hat{\mathbf{d}} \times \partial_\rho \hat{\mathbf{d}})$ , then[71, 73]

$$N_h = - \int d^2k d\theta \mathbf{j} \cdot \mathbf{A}. \quad (7)$$

It is found that  $N_h = n$  in our model[82]. We will call the topological defects defined by Eq.(6) as *Hopf defects*.

The more familiar Chern number, which characterizes 2D topological superconductors, is defined as[1, 31, 83]  $C(\lambda) = \frac{1}{2\pi} \int d^2k \epsilon^{ij} \partial_i a_j$  ( $i, j = k_x, k_y$ ). By straightforward calculations, we can see that  $C(\lambda) = 0$  for every  $\lambda$ , thus the uniform superconductor is topologically trivial.

Let us come back to Eq.(6) and focus on the  $n = 1$  defect first. We transform the Bloch Hamiltonian back to real-space lattice, then numerically solve the spectrum and eigenfunctions. Energy eigenvalues close to zero are shown in the inset of Fig.2, indicating the existence of two Majorana zero modes. One of the Majorana zero modes is sharply localized around the defect (Fig.2), the other is localized at the system edge (around  $\theta = 0$ ). Inspection of the wavefunctions indicates that they are equal-weight superpositions of the particle ( $\tau_z = 1$ ) and hole ( $\tau_z = -1$ ) components. The profiles of the  $\tau_z = 1$  and  $\tau_z = -1$  components are the same as shown in Fig.2 except that the heights are halved (thus there is no need to show them here). We emphasize that the BdG Hamiltonian with any

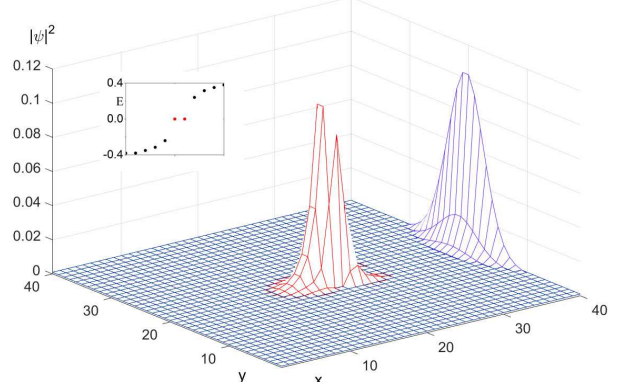


FIG. 2. The profiles of the two Majorana zero modes for the Hopf defect with  $N_h = 1$ . The inset shows several energies close to 0, with two zero energies colored in red.

fixed  $\theta$  is topologically trivial, yet the defect is nontrivial, as characterized by the Hopf invariant.

For  $n = 2$ , we find no zero mode in the defect, thus it is the  $Z_2$  Hopf invariant (even/odd) that determines the existence of Majorana zero mode.

*Edge theory.*—To gain intuitive understandings of the zero mode, we study the edge theory, looking for traces of zero mode. First, we numerically solved the edge states in open-boundary systems for various values of  $\lambda$ , and found that gapless edge modes exist only for  $\lambda = 0$ . In Fig.3a, we show the energy bands for a ribbon along  $y$  direction. The gapless edge modes for  $\lambda = 0$  are shown as the solid blue lines. They are non-chiral, and are immediately gapped out when  $\lambda$  is tuned away from 0 (edge modes of  $\lambda = \pi/20$  are shown in dashed curves), in other words, the edge modes are not topologically robust. This is consistent with the vanishing of Chern number.

This numerical observation is confirmed by analytic solutions. We consider a semi-infinite geometry with the sample occupying  $x < 0$  region,  $k_y$  being a good quantum number. For  $\lambda = 0$ , we obtain two degenerate edge modes at  $k_y = 0$ , both of which are eigenfunctions of  $\tau_x$  with eigenvalue  $-1$ [82], thus they are equal-weight superpositions of particle and hole components. We introduce Pauli matrices  $\sigma_{x,y,z}$  in this two-dimensional space, so that the two eigenfunctions have  $\sigma_z = \pm 1$ , respectively. Including small  $k_y$  and  $\lambda$  as perturbations, we derive an effective theory[82]:

$$H_{\text{eff}}(k_y, \lambda) = -vk_y \sigma_x + M\lambda \sigma_y, \quad (8)$$

where the effective parameters  $v, M$  are found to be both  $3/4$  in our specific model[82]. Thus the edge-state spectra are  $E_\pm(k_y) = \pm \sqrt{v^2 k_y^2 + M^2 \lambda^2}$ . It is immediately clear that the edge states become gapped when  $\lambda$  is tuned away from 0, which is consistent with the numerical finding in Fig.3a. As a comparison, we note that the edge spectrum of a chiral superconductor[1],  $E(k_y) = vk_y$ , cannot be gapped out.

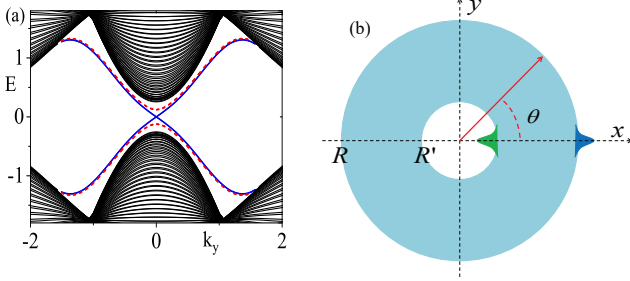


FIG. 3. (a) The energy bands for a ribbon with size  $L_x \times L_y = 40 \times \infty$ ;  $\lambda = 0$  (solid curves). The two dashed curves show the gapped edge modes for  $\lambda = \pi/20$  as a comparison. Each edge-mode band is doubly degenerate because a ribbon has two boundaries (ignoring a small splitting that exponentially decays as a function of  $L_x$ ). (b) A large hollow disk with two zero modes illustrated. The inner zero mode persists as the inner radius  $R' \rightarrow 0$ , evolving to the defect zero mode protected by Hopf invariant.

Based on this effective edge theory, we proceed to study a hollow disk with polar-angle-dependent parameter,  $\lambda = \theta$  (Fig.3b). We are only concerned with low-energy modes, therefore, we focus on the neighborhood of  $\theta = 0$ . Suppose that both the outer and inner radii  $R, R'$  are large. On the outer boundary, we have  $\lambda = \theta = y/R$ , thus the edge state spectra are given by solving  $H_{\text{eff}}(k_y \rightarrow -i\partial_y, \lambda \rightarrow y/R)\psi = E\psi$ . More explicitly, it reads

$$[iv\sigma_x\partial_y + (M/R)y\sigma_y]\psi = E\psi, \quad (9)$$

which squares to  $(-v^2\partial_y^2 + M^2y^2/R^2 - vM/R\sigma_z)\psi = E^2\psi$ . This equation resembles the Schrödinger equation of harmonic oscillators, though  $E$  is replaced by  $E^2$ , and there is a crucial additional  $-vM/R\sigma_z$  term. The eigenfunctions are  $\sigma_z$ -eigenvectors (eigenvalues are denoted by  $s_z = \pm 1$ ), with energies given by

$$E_{\text{outer}}^2(s_z, n) = 2(n + 1/2)vM/R - s_zvM/R, \quad (10)$$

where  $n = 0, 1, \dots$ . There is a zero mode in the  $s_z = +1$  sector, with  $n = 0$ , which is illustrated as the blue bump in Fig.3b. Since this mode is the eigenfunction of  $\tau_x$ , it is an equal superposition of particle and hole components.

For a semi-infinite geometry with sample occupying the  $x > 0$  region, the effective edge theory is almost the same as Eq.(8), except that the sign of the first term reversed[82]. On the inner boundary of the hollow disk (again near  $\theta = 0$ ), we have  $\lambda = \theta = y/R'$ , thus the edge-mode spectrum can be obtained from  $[-iv\sigma_x\partial_y + (M/R')y\sigma_y]\psi = E\psi$ , analogous to Eq.(9). The energies are given by

$$E_{\text{inner}}^2(s_z, n) = 2(n + 1/2)vM/R' + s_zvM/R', \quad (11)$$

which features a zero mode in the  $s_z = -1$  sector. The zero-mode wavefunction is

$$\psi_{\text{inner}} \sim \exp(-My^2/2vR')|s_z = -1\rangle, \quad (12)$$

which is exponentially localized near  $y = 0$ , namely  $\theta = 0$  (illustrated by the green bump in Fig.3b). All nonzero energies grow as  $1/R'$  as  $R'$  is decreased, while the zero mode remains at zero energy, evolving to the defect mode shown in Fig.2. For a hollow disk with  $\lambda = 2\theta$ , there are two zero modes on the inner boundary for large  $R'$ , near  $\theta = 0$  and  $\theta = \pi$ , respectively. Shrinking  $R'$  causes overlapping between them, which splits the two zero energies to nonzero values. This is consistent with the absence of zero mode in the  $n = 2$  defect.

It is useful to compare our systems with the  $p$ -wave chiral topological superconductor[1], for which a magnetic vortex hosts a zero mode. The chiral superconductor is topologically nontrivial, while the superconductors in our model for any  $\lambda$  is topologically trivial. There are robust gapless edge states in chiral superconductors, while gapless edge modes appear only for  $\lambda = 0$  in our model, moreover, these non-chiral edge modes can be gapped out by perturbations. For chiral superconductor on a hollow-disk geometry with a unit magnetic flux, the zero mode wavefunction is evenly distributed on the boundary circle[1, 84], while the zero mode in our model is exponentially localized near  $\theta = 0$  (Fig.3b).

**T-junctions.**—So far, we have only studied configurations with  $\lambda$  continuously varied. It is conceivable that the continuous function  $\lambda(\theta) = \theta$  can be replaced by a discontinuous one, for instance, we may consider a T-junction:

$$\lambda(\theta) = \begin{cases} \lambda_1, & \theta \in [0, \pi/2] \\ \lambda_2, & \theta \in [\pi/2, \pi] \\ \lambda_3, & \theta \in [\pi, 2\pi]. \end{cases} \quad (13)$$

$\lambda_{1,2,3}$  being three unequal constants.

We will study the simpler superconductor-superconductor-vacuum T-junction by replacing the  $\lambda_3$ -region by the vacuum. Since the value of  $\lambda$  in the vacuum is not well defined, this replacement is not fully justified in advance. Nevertheless, the numerical results thus obtained indicate that Majorana zero modes do exist in such T-junctions, as shown in Fig.4a for  $\lambda_1 = 0.1\pi$ ,  $\lambda_2 = \pi$ . There is certain arbitrariness in choosing the hopping at the boundary between the  $\lambda_{1,2}$  regions, for which we keep only the nearest-neighbor hopping (discarding the next-nearest-neighbor hopping and the pairing)[85]. The energy eigenvalues near zero are shown in Fig.4c (we show 12 of them), from which it is clear that the zero-mode levels are separate from all other energy levels by a finite gap in the  $L \rightarrow \infty$  limit.

We have also studied superconductor-insulator-vacuum T-junctions. To this end, we consider the  $H_\eta$  in Eq.(5), in which taking  $\eta = 0$  amounts to removing the Cooper pairing. We notice that  $H_{\eta=0}(\mathbf{k}, \lambda = \pi)$  describes an insulator without any Fermi surface [In contrast,  $H_{\eta=0}(\mathbf{k}, \lambda = 0.1\pi)$  describes a metal]. Now we can design superconductor-insulator-vacuum T-junctions by taking  $\eta = 1$  in the  $\lambda_1 = 0.1\pi$  region, and  $\eta = 0$  in the  $\lambda_2 = \pi$  region. We find one Majorana zero mode for each T-junction (shown in Fig.4b), and the energy gap between the zero-mode levels and other energy levels is apparent in Fig.4d. We emphasize that each region by itself is topologically trivial, in particular, the superconductor (with  $\lambda = 0.1\pi$ )

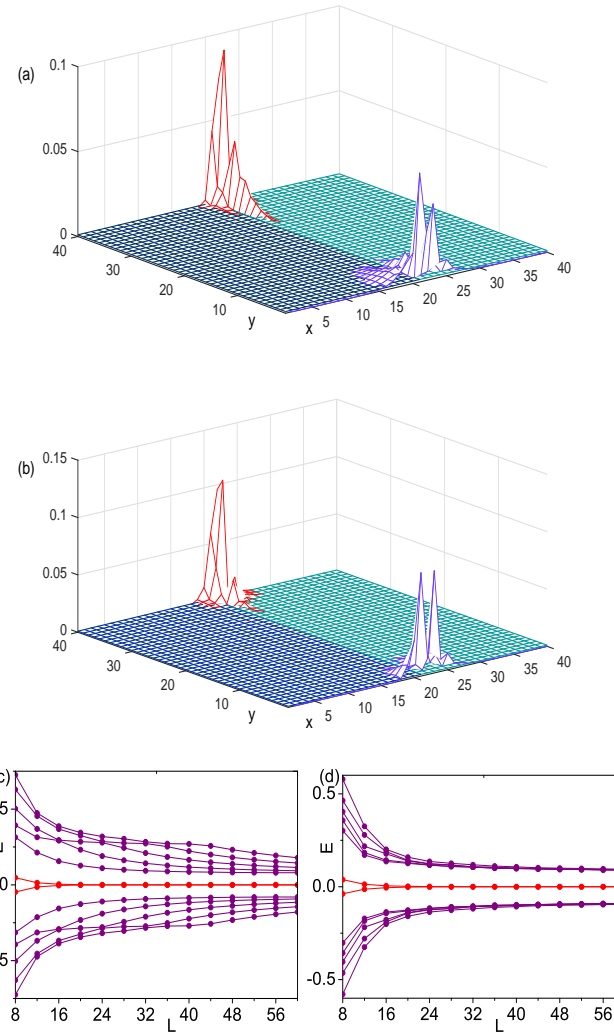


FIG. 4. (a) Superconductor-superconductor-vacuum T-junctions. The system size is  $L^2$ , with  $L = 40$ . The  $x > L/2$  and  $x \leq L/2$  region, shown in different colors, is described by Eq.(2) with  $\lambda$  taking  $\lambda_1 = 0.1\pi$  and  $\lambda_2 = \pi$ , respectively. The peaks are the profiles of the two Majorana zero modes localized around the two T-junctions (each T-junction hosts one mode). (b) Superconductor-insulator-vacuum T-junctions. The parameters are the same as (a) except that  $d_x$  and  $d_y$  are tuned to 0 in the  $\lambda_2$  region, so that  $\lambda_2$  region is an insulator. (c) and (d) shows 12 energies closest to 0, for system (a) and (b), respectively.

is a topologically trivial one without gapless edge state.

*Conclusions.*—We have investigated the intriguing possibility of creating Majorana zero modes in 2D topologically trivial superconductors. The Hopf defect made of trivial superconductors is studied as a concrete example. Furthermore, we studied the more accessible T-junctions constructed from topologically trivial superconductors. Hopefully, the trivial-superconductor-based approach will broaden the scope of searching Majorana zero modes in various superconductors. In particular, absence of chiral Majorana edge state in a 2D superconducting sample does not necessarily imply absence

of robust Majorana zero mode in its point defects.

We conclude with several remarks. First, we have focused on a single-band model, while real materials usually have multi-bands. We emphasize that the zero modes found here are nevertheless robust to small mixing with other bands: a single zero eigenvalue cannot be shifted away from zero due to the intrinsic particle-hole symmetry of the BdG equation. Second, we have taken a simple model BdG Hamiltonians as our starting point (like Ref.[1]). More realistic Hamiltonians should be adopted when coping with real materials, for instance, the semiconductor-superconductor heterostructures[28, 29], for which our theory implies that robust Majorana zero modes can exist in appropriate defects (e.g. judiciously constructed T-junctions), without requiring the uniform system being tuned to the topologically nontrivial regime. This will be left for future works.

*Acknowledgements.*—This work is supported by NSFC (No. 11674189). Z.Y. is supported in part by China Postdoctoral Science Foundation (No. 2016M590082).

\* wangzhongemail@tsinghua.edu.cn

- [1] N. Read and Dmitry Green, “Paired states of fermions in two dimensions with breaking of parity and time-reversal symmetries and the fractional quantum hall effect,” *Phys. Rev. B* **61**, 10267–10297 (2000).
- [2] GE Volovik, “Fermion zero modes on vortices in chiral superconductors,” *Journal of Experimental and Theoretical Physics Letters* **70**, 609–614 (1999).
- [3] M. Z. Hasan and C. L. Kane, “*Colloquium : Topological insulators*,” *Rev. Mod. Phys.* **82**, 3045–3067 (2010).
- [4] Xiao-Liang Qi and Shou-Cheng Zhang, “Topological insulators and superconductors,” *Rev. Mod. Phys.* **83**, 1057–1110 (2011).
- [5] A. Bansil, Hsin Lin, and Tanmoy Das, “*Colloquium : Topological band theory*,” *Rev. Mod. Phys.* **88**, 021004 (2016).
- [6] B Andrei Bernevig and Taylor L Hughes, *Topological insulators and topological superconductors* (Princeton University Press, 2013).
- [7] Shun-Qing Shen, *Topological Insulators: Dirac Equation in Condensed Matters*, Vol. 174 (Springer Science & Business Media, 2013).
- [8] A Yu Kitaev, “Unpaired majorana fermions in quantum wires,” *Physics-Uspekhi* **44**, 131 (2001).
- [9] Chetan Nayak, Steven H. Simon, Ady Stern, Michael Freedman, and Sankar Das Sarma, “Non-abelian anyons and topological quantum computation,” *Rev. Mod. Phys.* **80**, 1083 (2008).
- [10] Gregory Moore and Nicholas Read, “Nonabelions in the fractional quantum hall effect,” *Nuclear Physics B* **360**, 362–396 (1991).
- [11] Xiao-Gang Wen, “Non-abelian statistics in the fractional quantum hall states,” *Physical review letters* **66**, 802 (1991).
- [12] D. A. Ivanov, “Non-abelian statistics of half-quantum vortices in  $p$ -wave superconductors,” *Phys. Rev. Lett.* **86**, 268–271 (2001).
- [13] Sankar Das Sarma, Michael Freedman, and Chetan Nayak, “Topologically protected qubits from a possible non-abelian fractional quantum hall state,” *Phys. Rev. Lett.* **94**, 166802 (2005).

[14] S. Vijay and L. Fu, “Braiding without Braiding: Teleportation-Based Quantum Information Processing with Majorana Zero Modes,” ArXiv e-prints (2016), arXiv:1609.00950 [cond-mat.mes-hall].

[15] Parsa Bonderson, Michael Freedman, and Chetan Nayak, “Measurement-only topological quantum computation,” Phys. Rev. Lett. **101**, 010501 (2008).

[16] David Aasen, Michael Hell, Ryan V. Mishmash, Andrew Higginbotham, Jeroen Danon, Martin Leijnse, Thomas S. Jespersen, Joshua A. Folk, Charles M. Marcus, Karsten Flensberg, and Jason Alicea, “Milestones toward majorana-based quantum computing,” Phys. Rev. X **6**, 031016 (2016).

[17] Torsten Karzig, Yuval Oreg, Gil Refael, and Michael H. Freedman, “Universal geometric path to a robust majorana magic gate,” Phys. Rev. X **6**, 031019 (2016).

[18] T. Karzig, C. Knapp, R. Lutchyn, P. Bonderson, M. Hastings, C. Nayak, J. Alicea, K. Flensberg, S. Plugge, Y. Oreg, C. Marcus, and M. H. Freedman, “Scalable Designs for Quasiparticle-Poisoning-Protected Topological Quantum Computation with Majorana Zero Modes,” ArXiv e-prints (2016), arXiv:1610.05289 [cond-mat.mes-hall].

[19] B Van Heck, AR Akhmerov, F Hassler, M Burrello, and CWJ Beenakker, “Coulomb-assisted braiding of majorana fermions in a josephson junction array,” New Journal of Physics **14**, 035019 (2012).

[20] L. A. Landau, S. Plugge, E. Sela, A. Altland, S. M. Albrecht, and R. Egger, “Towards realistic implementations of a majorana surface code,” Phys. Rev. Lett. **116**, 050501 (2016).

[21] Jason Alicea, “New directions in the pursuit of majorana fermions in solid state systems,” Reports on Progress in Physics **75**, 076501 (2012).

[22] C. W. J. Beenakker, “Search for Majorana Fermions in Superconductors,” Annual Review of Condensed Matter Physics **4**, 113–136 (2013).

[23] Tudor D Stanescu and Sumanta Tewari, “Majorana fermions in semiconductor nanowires: fundamentals, modeling, and experiment,” Journal of Physics: Condensed Matter **25**, 233201 (2013).

[24] Martin Leijnse and Karsten Flensberg, “Introduction to topological superconductivity and majorana fermions,” Semiconductor Science and Technology **27**, 124003 (2012).

[25] Steven R. Elliott and Marcel Franz, “Colloquium : Majorana fermions in nuclear, particle, and solid-state physics,” Rev. Mod. Phys. **87**, 137–163 (2015).

[26] Sankar Das Sarma, Michael Freedman, and Chetan Nayak, “Majorana zero modes and topological quantum computation,” npj Quantum Information **1**, 15001 (2015).

[27] Masatoshi Sato and Satoshi Fujimoto, “Majorana fermions and topology in superconductors,” Journal of the Physical Society of Japan **85**, 072001 (2016).

[28] Jay D. Sau, Roman M. Lutchyn, Sumanta Tewari, and S. Das Sarma, “Generic new platform for topological quantum computation using semiconductor heterostructures,” Phys. Rev. Lett. **104**, 040502 (2010).

[29] Jason Alicea, “Majorana fermions in a tunable semiconductor device,” Phys. Rev. B **81**, 125318 (2010).

[30] Liang Fu and C. L. Kane, “Superconducting proximity effect and majorana fermions at the surface of a topological insulator,” Phys. Rev. Lett. **100**, 096407 (2008).

[31] Xiao-Liang Qi, Taylor L. Hughes, and Shou-Cheng Zhang, “Chiral topological superconductor from the quantum hall state,” Phys. Rev. B **82**, 184516 (2010).

[32] Suk Bum Chung, Xiao-Liang Qi, Joseph Maciejko, and Shou-Cheng Zhang, “Conductance and noise signatures of majorana backscattering,” Phys. Rev. B **83**, 100512 (2011).

[33] K. T. Law, Patrick A. Lee, and T. K. Ng, “Majorana fermion induced resonant andreev reflection,” Phys. Rev. Lett. **103**, 237001 (2009).

[34] A. R. Akhmerov, Johan Nilsson, and C. W. J. Beenakker, “Electrically detected interferometry of majorana fermions in a topological insulator,” Phys. Rev. Lett. **102**, 216404 (2009).

[35] Yuval Oreg, Gil Refael, and Felix von Oppen, “Helical liquids and majorana bound states in quantum wires,” Phys. Rev. Lett. **105**, 177002 (2010).

[36] Roman M. Lutchyn, Jay D. Sau, and S. Das Sarma, “Majorana fermions and a topological phase transition in semiconductor-superconductor heterostructures,” Phys. Rev. Lett. **105**, 077001 (2010).

[37] Jason Alicea, Yuval Oreg, Gil Refael, Felix von Oppen, and Matthew PA Fisher, “Non-abelian statistics and topological quantum information processing in 1d wire networks,” Nature Physics **7**, 412–417 (2011).

[38] Roman M. Lutchyn, Tudor D. Stanescu, and S. Das Sarma, “Search for majorana fermions in multiband semiconducting nanowires,” Phys. Rev. Lett. **106**, 127001 (2011).

[39] Tudor D. Stanescu, Roman M. Lutchyn, and S. Das Sarma, “Majorana fermions in semiconductor nanowires,” Phys. Rev. B **84**, 144522 (2011).

[40] Andrew C. Potter and Patrick A. Lee, “Multichannel generalization of kitaev’s majorana end states and a practical route to realize them in thin films,” Phys. Rev. Lett. **105**, 227003 (2010).

[41] S. Das Sarma, Jay D. Sau, and Tudor D. Stanescu, “Splitting of the zero-bias conductance peak as smoking gun evidence for the existence of the majorana mode in a superconductor-semiconductor nanowire,” Phys. Rev. B **86**, 220506 (2012).

[42] M. Wimmer, A. R. Akhmerov, M. V. Medvedyeva, J. Tworzydlo, and C. W. J. Beenakker, “Majorana bound states without vortices in topological superconductors with electrostatic defects,” Phys. Rev. Lett. **105**, 046803 (2010).

[43] Masatoshi Sato, Yoshiro Takahashi, and Satoshi Fujimoto, “Non-abelian topological order in *s*-wave superfluids of ultracold fermionic atoms,” Phys. Rev. Lett. **103**, 020401 (2009).

[44] Chuanwei Zhang, Sumanta Tewari, Roman M. Lutchyn, and S. Das Sarma, “ $p_x + ip_y$  superfluid from *s*-wave interactions of fermionic cold atoms,” Phys. Rev. Lett. **101**, 160401 (2008).

[45] Sumanta Tewari, S Das Sarma, Chetan Nayak, Chuanwei Zhang, and P Zoller, “Quantum computation using vortices and majorana zero modes of a  $p$   $p$   $x + i p y$  superfluid of fermionic cold atoms,” Physical review letters **98**, 010506 (2007).

[46] Xiong-Jun Liu, K. T. Law, and T. K. Ng, “Realization of 2d spin-orbit interaction and exotic topological orders in cold atoms,” Phys. Rev. Lett. **112**, 086401 (2014).

[47] Liang Jiang, Takuya Kitagawa, Jason Alicea, A. R. Akhmerov, David Pekker, Gil Refael, J. Ignacio Cirac, Eugene Demler, Mikhail D. Lukin, and Peter Zoller, “Majorana fermions in equilibrium and in driven cold-atom quantum wires,” Phys. Rev. Lett. **106**, 220402 (2011).

[48] Sebastian Diehl, Enrique Rico, Mikhail A Baranov, and Peter Zoller, “Topology by dissipation in atomic quantum wires,” Nature Physics **7**, 971–977 (2011).

[49] Vincent Mourik, Kun Zuo, Sergey M Frolov, SR Plissard, EPAM Bakkers, and LP Kouwenhoven, “Signatures of majorana fermions in hybrid superconductor-semiconductor nanowire devices,” Science **336**, 1003–1007 (2012).

[50] Stevan Nadj-Perge, Ilya K Dordzov, Jian Li, Hua Chen, Sangjun Jeon, Jungpil Seo, Allan H MacDonald, B Andrei Bernevig, and Ali Yazdani, “Observation of majorana fermions in fer-

romagnetic atomic chains on a superconductor," *Science* **346**, 602–607 (2014).

[51] Leonid P Rokhinson, Xinyu Liu, and Jacek K Furdyna, "The fractional ac josephson effect in a semiconductor-superconductor nanowire as a signature of majorana particles," *Nature Physics* **8**, 795–799 (2012).

[52] MT Deng, CL Yu, GY Huang, Marcus Larsson, Philippe Caroff, and HQ Xu, "Anomalous zero-bias conductance peak in a nb-insb nanowire-nb hybrid device," *Nano letters* **12**, 6414–6419 (2012).

[53] Anindya Das, Yuval Ronen, Yonatan Most, Yuval Oreg, Moty Heiblum, and Hadas Shtrikman, "Zero-bias peaks and splitting in an al-inas nanowire topological superconductor as a signature of majorana fermions," *Nature Physics* **8**, 887–895 (2012).

[54] A. D. K. Finck, D. J. Van Harlingen, P. K. Mohseni, K. Jung, and X. Li, "Anomalous modulation of a zero-bias peak in a hybrid nanowire-superconductor device," *Phys. Rev. Lett.* **110**, 126406 (2013).

[55] HOH Churchill, V Fatemi, Kasper Grove-Rasmussen, MT Deng, Philippe Caroff, HQ Xu, and Charles M Marcus, "Superconductor-nanowire devices from tunneling to the multichannel regime: Zero-bias oscillations and magnetoconductance crossover," *Physical Review B* **87**, 241401 (2013).

[56] SM Albrecht, AP Higginbotham, M Madsen, F Kuemmeth, TS Jespersen, Jesper Nygård, P Krogstrup, and CM Marcus, "Exponential protection of zero modes in majorana islands," *Nature* **531**, 206–209 (2016).

[57] MT Deng, S Vaitiekėnas, EB Hansen, J Danon, M Leijnse, K Flensberg, J Nygård, P Krogstrup, and CM Marcus, "Majorana bound state in a coupled quantum-dot hybrid-nanowire system," *Science* **354**, 1557–1562 (2016).

[58] Marcel Franz, "Majorana's wires," *Nature nanotechnology* **8**, 149–152 (2013).

[59] Jin-Peng Xu, Mei-Xiao Wang, Zhi Long Liu, Jian-Feng Ge, Xiaojun Yang, Canhua Liu, Zhu An Xu, Dandan Guan, Chun Lei Gao, Dong Qian, Ying Liu, Qiang-Hua Wang, Fu-Chun Zhang, Qi-Kun Xue, and Jin-Feng Jia, "Experimental detection of a majorana mode in the core of a magnetic vortex inside a topological insulator-superconductor  $\text{bi}_2\text{te}_3/\text{nbse}_2$  heterostructure," *Phys. Rev. Lett.* **114**, 017001 (2015).

[60] Hao-Hua Sun, Kai-Wen Zhang, Lun-Hui Hu, Chuang Li, Guan-Yong Wang, Hai-Yang Ma, Zhu-An Xu, Chun-Lei Gao, Dan-Dan Guan, Yao-Yi Li, Canhua Liu, Dong Qian, Yi Zhou, Liang Fu, Shao-Chun Li, Fu-Chun Zhang, and Jin-Feng Jia, "Majorana zero mode detected with spin selective andreev reflection in the vortex of a topological superconductor," *Phys. Rev. Lett.* **116**, 257003 (2016).

[61] Y.-F. Lv, W.-L. Wang, Y.-M. Zhang, H. Ding, W. Li, L. Wang, K. He, C.-L. Song, X.-C. Ma, and Q.-K. Xue, "Experimental Observation of Topological Superconductivity and Majorana Zero Modes on beta-Bi2Pd Thin Films," *ArXiv e-prints* (2016), arXiv:1607.07551 [cond-mat.supr-con].

[62] Mei-Xiao Wang, Canhua Liu, Jin-Peng Xu, Fang Yang, Lin Miao, Meng-Yu Yao, CL Gao, Chenyi Shen, Xucun Ma, X Chen, *et al.*, "The coexistence of superconductivity and topological order in the  $\text{bi}_2\text{se}_3$  thin films," *Science* **336**, 52–55 (2012).

[63] ZF Wang, Huimin Zhang, Defa Liu, Chong Liu, Chenjia Tang, Canli Song, Yong Zhong, Junping Peng, Fangsen Li, Caina Nie, LiLi Wang, X. J. Zhou, Xucun Ma, Q. K. Xue, and Feng Liu, "Topological edge states in a high-temperature superconductor fese/srtio3 (001) film," *Nature Materials* **15**, 968–973 (2016).

[64] Q. L. He, L. Pan, A. L. Stern, E. Burks, X. Che, G. Yin, J. Wang, B. Lian, Q. Zhou, E. S. Choi, K. Murata, X. Kou, T. Nie, Q. Shao, Y. Fan, S.-C. Zhang, K. Liu, J. Xia, and K. L. Wang, "Chiral Majorana edge state in a quantum anomalous Hall insulator-superconductor structure," *ArXiv e-prints* (2016), arXiv:1606.05712 [cond-mat.supr-con].

[65] J. C. Y. Teo and C. L. Kane, "Topological defects and gapless modes in insulators and superconductors," *Phys. Rev. B* **82**, 115120 (2010).

[66] Ching-Kai Chiu, Jeffrey C. Y. Teo, Andreas P. Schnyder, and Shinsei Ryu, "Classification of topological quantum matter with symmetries," *Rev. Mod. Phys.* **88**, 035005 (2016).

[67] Ken Shiozaki and Masatoshi Sato, "Topology of crystalline insulators and superconductors," *Phys. Rev. B* **90**, 165114 (2014).

[68] Dung-Hai Lee, Guang-Ming Zhang, and Tao Xiang, "Edge solitons of topological insulators and fractionalized quasiparticles in two dimensions," *Phys. Rev. Lett.* **99**, 196805–4 (2007).

[69] Xiao-Liang Qi, Taylor Hughes, and Shou-Cheng Zhang, "Fractional charge and quantized current in the quantum spin Hall state," *Nature Physics* **4**, 273 (2008).

[70] Ying Ran, Yi Zhang, and Ashvin Vishwanath, "One-dimensional topologically protected modes in topological insulators with lattice dislocations," *Nature Physics* **5**, 298–303 (2009).

[71] Frank Wilczek and A. Zee, "Linking numbers, spin, and statistics of solitons," *Phys. Rev. Lett.* **51**, 2250–2252 (1983).

[72] Eduardo Fradkin, *Field theories of condensed matter physics* (Cambridge University Press, 2013).

[73] Joel E Moore, Ying Ran, and Xiao-Gang Wen, "Topological surface states in three-dimensional magnetic insulators," *Physical review letters* **101**, 186805 (2008).

[74] D.-L. Deng, S.-T. Wang, C. Shen, and L.-M. Duan, "Hopf insulators and their topologically protected surface states," *Phys. Rev. B* **88**, 201105 (2013).

[75] D.-L. Deng, S.-T. Wang, and L.-M. Duan, "Systematic construction of tight-binding hamiltonians for topological insulators and superconductors," *Phys. Rev. B* **89**, 075126 (2014).

[76] D.-L. Deng, S.-T. Wang, K. Sun, and L.-M. Duan, "Probe knots and Hopf insulators with ultracold atoms," *ArXiv e-prints* (2016), arXiv:1612.01518 [cond-mat.mes-hall].

[77] Ricardo Kennedy, "Topological hopf-chern insulators and the hopf superconductor," *Phys. Rev. B* **94**, 035137 (2016).

[78] C. Liu, F. Vafa, and C. Xu, "Symmetry Protected Topological Hopf Insulator and its Generalizations," *ArXiv e-prints* (2016), arXiv:1612.04905 [cond-mat.str-el].

[79] C. Wang, P. Zhang, X. Chen, J. Yu, and H. Zhai, "Measuring Topological Number of a Chern-Insulator from Quench Dynamics," *ArXiv e-prints* (2016), arXiv:1611.03304 [cond-mat.quant-gas].

[80] N. Fläschner, D. Vogel, M. Tarnowski, B. S. Rem, D.-S. Lühmann, M. Heyl, J. C. Budich, L. Mathey, K. Sengstock, and C. Weitenberg, "Observation of a dynamical topological phase transition," *ArXiv e-prints* (2016), arXiv:1608.05616 [cond-mat.quant-gas].

[81] Converting a momentum variable to an angle variable was adopted in Refs.[65, 86].

[82] Supplemental Material.

[83] D. J. Thouless, M. Kohmoto, M. P. Nightingale, and M. den Nijs, "Quantized hall conductance in a two-dimensional periodic potential," *Phys. Rev. Lett.* **49**, 405–408 (1982).

[84] Paul Fendley, Matthew P. A. Fisher, and Chetan Nayak, "Edge states and tunneling of non-abelian quasiparticles in the  $\nu = 5/2$  quantum hall state and  $p + ip$  superconductors," *Phys. Rev. B* **75**, 045317 (2007).

[85] Keeping only the nearest-neighbor hopping means that (in real space)  $H_{rs} = (1.5 - \cos \lambda) \tau_z$  for the boundary sites  $\mathbf{r} = (L/2, y)$  and  $\mathbf{s} = (L/2 + 1, y)$ , where we take  $\lambda$  as  $\lambda_2 = \pi$  (Another choice can be  $\lambda = \lambda_1$ . The choice is not unique).

[86] Xiao-Liang Qi, Taylor Hughes, and Shou-Cheng Zhang, “Topological Field Theory of Time-Reversal Invariant Insulators,” Phys. Rev. B **78**, 195424 (2008).

## Supplemental Material

### I. EXPLICIT EXPRESSIONS OF $d_{x,y,z}$

In the main article, we have taken  $d_i = z^\dagger \tau_i z$  with  $z = (z_\uparrow, z_\downarrow)^T$  and

$$\begin{aligned} z_\uparrow &= \sin k_x + i \sin k_y, \\ z_\downarrow &= \sin \lambda + i[\cos k_x + \cos k_y + \cos \lambda - \frac{3}{2}], \end{aligned} \quad (14)$$

In explicit form, these  $d_i$ ’s read

$$\begin{aligned} d_x &= 2 \sin k_x \sin \lambda + 2 \sin k_y \cos k_x + \sin 2k_y + 2 \sin k_y \cos \lambda \\ &\quad - 3 \sin k_y, \\ d_y &= -2 \sin k_y \sin \lambda + 2 \sin k_x \cos k_y + \sin 2k_x + 2 \sin k_x \cos \lambda \\ &\quad - 3 \sin k_x, \\ d_z &= -\frac{13}{4} - \cos 2k_x - \cos 2k_y - 2 \cos k_x \cos k_y - 2 \cos k_x \cos \lambda \\ &\quad - 2 \cos k_y \cos \lambda + 3(\cos k_x + \cos k_y + \cos \lambda). \end{aligned} \quad (15)$$

### II. NUMERICAL CALCULATION OF HOPF INVARIANT

For generality, we have also considered multiplying the Cooper pairing terms  $d_x \tau_x$  and  $d_y \tau_y$  in the Hamiltonian by a factor  $\eta$ :

$$H_\eta \equiv \sum_i \tilde{d}_i \tau_i = \eta(d_x \tau_x + d_y \tau_y) + d_z \tau_z, \quad (16)$$

For  $\eta \ll 1$ ,  $H_\eta$  describes a superconductor with weak pairing (in the main article, we focused on the  $\eta = 1$  case).

The Hopf invariant, which characterizes the topological property of the Hamiltonian, is given by

$$N_h = - \int d^2k d\theta \mathbf{j}(\mathbf{k}, \theta) \cdot \mathbf{A}(\mathbf{k}, \theta), \quad (17)$$

where  $\mathbf{j}(\mathbf{k}, \theta) = (j^x, j^y, j^\theta)$  (Note that the superscripts  $x, y$  stand for  $k_x, k_y$  takes the form of

$$j^\mu = \frac{1}{8\pi} \epsilon^{\mu\nu\rho} \hat{d} \cdot (\partial_\nu \hat{d} \times \partial_\rho \hat{d}) \quad (18)$$

with

$$\hat{d} = \frac{(\tilde{d}_x, \tilde{d}_y, \tilde{d}_z)}{\sqrt{\tilde{d}_x^2 + \tilde{d}_y^2 + \tilde{d}_z^2}}, \quad (19)$$

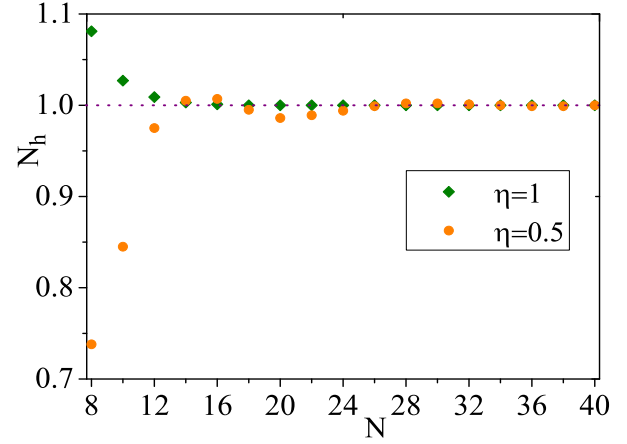


FIG. 5. Numerical results of the Hopf invariant for  $\eta = 1$  and  $\eta = 0.5$  ( $n = 1$ ). As the Brillouin zone grid becomes finer,  $N_h$  converges rapidly to 1.

and  $\mathbf{A} = (A^x, A^y, A^\theta)$  (again, the superscripts  $x, y$  stand for  $k_x, k_y$ ) is the gauge potential satisfying  $\nabla \times \mathbf{A} = \mathbf{j}$ , where  $\nabla = (\partial/\partial k_x, \partial/\partial k_y, \partial/\partial \theta)$ . It is difficult to do the integration in Eq.(17) analytically. To do it numerically, we rewrite Eq(17) into a discrete form:

$$N_h = -\frac{(2\pi)^3}{N^3} \sum_{\mathbf{k}, \theta} \mathbf{j}(\mathbf{k}, \theta) \cdot \mathbf{A}(\mathbf{k}, \theta), \quad (20)$$

where  $N$  is the number of lattice sites (the lattice constant is set to unit) and  $k_x, k_y, \theta$  take discrete values in  $\{-\pi, -\pi + \frac{2\pi}{N}, \dots, \pi - \frac{2\pi}{N}\}$ .

To obtain the expression of  $\mathbf{A}$  from  $\mathbf{j}$ , we do the following Fourier transformation:

$$\begin{aligned} \mathbf{A}(\mathbf{k}, \theta) &= \frac{1}{N^{3/2}} \sum_{\mathbf{q}} \mathbf{A}(\mathbf{q}) e^{-i(q_x k_x + q_y k_y + q_\theta \theta)}, \\ \mathbf{j}(\mathbf{k}, \theta) &= \frac{1}{N^{3/2}} \sum_{\mathbf{q}} \mathbf{j}(\mathbf{q}) e^{-i(q_x k_x + q_y k_y + q_\theta \theta)}, \end{aligned} \quad (21)$$

where  $\mathbf{q} = (q_x, q_y, q_\theta)$ , whose components  $q_{x,y,\theta}$  take discrete values in  $\{-\frac{N}{2}, -\frac{N}{2} + 1, \dots, \frac{N}{2} - 1\}$ . Under the gauge  $\mathbf{q} \cdot \mathbf{A} = 0$ , it is readily found that

$$\mathbf{A}(\mathbf{q}) = -i \frac{\mathbf{q} \times \mathbf{j}(\mathbf{q})}{\mathbf{q}^2}, \quad (22)$$

thus the Hopf invariant becomes

$$\begin{aligned} N_h &= -\frac{(2\pi)^3}{N^3} \sum_{\mathbf{q}} \mathbf{j}(-\mathbf{q}) \cdot \mathbf{A}(\mathbf{q}) \\ &= i \frac{(2\pi)^3}{N^3} \sum_{\mathbf{q}} \frac{\mathbf{j}(-\mathbf{q}) \cdot (\mathbf{q} \times \mathbf{j}(\mathbf{q}))}{\mathbf{q}^2}. \end{aligned} \quad (23)$$

The numerical integration converges quite rapidly as we increase  $N$ . For  $\lambda = n\theta$ , we find  $N_h = n$ . The  $n = 1$  case is shown in Fig.5.

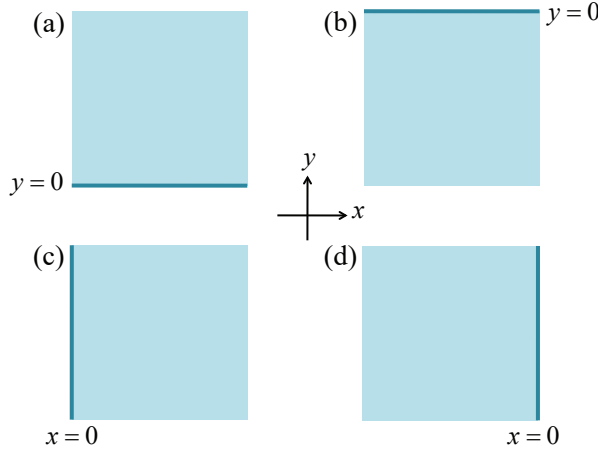


FIG. 6. Four geometries of the sample. The sample occupies (a) the  $y > 0$  region, (b) the  $y < 0$  region, (c) the  $x > 0$  region, (d) the  $x < 0$  region.

### III. EDGE THEORY FOR VARIOUS SYSTEM GEOMETRIES

Sample occupying  $y > 0$

First, we study a semi-infinite geometry with the sample occupying the  $y > 0$  region (illustrated in Fig. 6(a)). The momentum  $k_x$  remains a good quantum number, while  $k_y$  is not. In the  $y$  direction, we use the real-space coordinate, which is an integer in our lattice model. The wave functions and energy eigenvalues can be obtained by solving the following equation

$$\begin{pmatrix} H_0 & H_1 & H_2 & 0 & 0 & 0 & \cdots \\ H_1^\dagger & H_0 & H_1 & H_2 & 0 & 0 & \cdots \\ H_2^\dagger & H_1^\dagger & H_0 & H_1 & H_2 & 0 & \cdots \\ 0 & H_2^\dagger & H_1^\dagger & H_0 & H_1 & H_2 & \cdots \\ \vdots & \vdots & \vdots & \vdots & \vdots & \vdots & \ddots \end{pmatrix} \begin{pmatrix} \psi_1 \\ \psi_2 \\ \psi_3 \\ \psi_4 \\ \vdots \end{pmatrix} = E \begin{pmatrix} \psi_1 \\ \psi_2 \\ \psi_3 \\ \psi_4 \\ \vdots \end{pmatrix}, \quad (24)$$

where the subscript  $j$  of  $\psi_j$  is the  $y$  coordinate, each  $\psi_j$  is two-component, and

$$\begin{aligned} H_0(k_x, \lambda) &= \begin{pmatrix} -\frac{13}{4} - \cos 2k_x + 3(\cos k_x + \cos \lambda) - 2 \cos k_x \cos \lambda & 2 \sin k_x \sin \lambda - i(\sin 2k_x + 2 \sin k_x \cos \lambda - 3 \sin k_x) \\ 2 \sin k_x \sin \lambda + i(\sin 2k_x + 2 \sin k_x \cos \lambda - 3 \sin k_x) & \frac{13}{4} + \cos 2k_x - 3(\cos k_x + \cos \lambda) + 2 \cos k_x \cos \lambda \end{pmatrix}, \\ H_1(k_x, \lambda) &= \begin{pmatrix} \frac{3}{2} - \cos k_x - \cos \lambda & -i(\cos k_x + \cos \lambda - \frac{3}{2}) - i \sin k_x + \sin \lambda \\ -i(\cos k_x + \cos \lambda - \frac{3}{2}) + i \sin k_x - \sin \lambda & -\frac{3}{2} + \cos k_x + \cos \lambda \end{pmatrix}, \\ H_2(k_x, \lambda) &= \begin{pmatrix} -\frac{1}{2} & -\frac{1}{2}i \\ -\frac{1}{2}i & \frac{1}{2} \end{pmatrix}. \end{aligned} \quad (25)$$

Eq.(24) can be written compactly as  $H(k_x, \lambda)|\Psi\rangle = E|\Psi\rangle$ ,  $H$  denoting the large matrix at the left-hand-side of Eq.(24). Let us first find the zero-energy ( $E = 0$ ) solutions, if any, at  $k_x = 0$  and  $\lambda = 0$ . When  $k_x = 0$  and  $\lambda = 0$ ,  $H_i$ 's simplify to

$$\begin{aligned} H_0(0, 0) &= \begin{pmatrix} -\frac{1}{4} & 0 \\ 0 & \frac{1}{4} \end{pmatrix}, \\ H_1(0, 0) = H_2(0, 0) &= \begin{pmatrix} -\frac{1}{2} & -\frac{1}{2}i \\ -\frac{1}{2}i & \frac{1}{2} \end{pmatrix}. \end{aligned} \quad (26)$$

We can define  $\tau_{\pm} = (\tau_z \pm i\tau_x)/2$ , which is the raising/lowering operator of  $\tau_y$ , thus  $H_0 = -(\tau_+ + \tau_-)/4$ ,  $H_1 = H_2 = -\tau_+$ , and  $H_1^\dagger = H_2^\dagger = -\tau_-$ . Operating on the  $\tau_y$  eigenvectors  $|\chi_{\pm}\rangle = (1, \pm i)^T/\sqrt{2}$ , they produce

$$\begin{aligned} H_1|\chi_+\rangle &= 0, H_1^\dagger|\chi_+\rangle = -|\chi_-\rangle; \\ H_1|\chi_-\rangle &= -|\chi_+\rangle, H_1^\dagger|\chi_-\rangle = 0; \\ H_0|\chi_+\rangle &= -\frac{1}{4}|\chi_-\rangle, H_0|\chi_-\rangle = \frac{1}{4}|\chi_+\rangle, \end{aligned} \quad (27)$$

We can check that the zero-energy wavefunctions take the form of

$$|\Psi\rangle = \sum_j a_j |j\rangle \otimes |\chi_-\rangle, \quad (28)$$

where  $|j\rangle$  is localized on the  $j$ -site:

$$|j\rangle = (\underbrace{0, 0, \dots, 0}_{j-1}, 1, 0, \dots)^T, \quad (29)$$

with the coefficients  $a_j$  satisfying the following iteration relation:

$$a_j = -4(a_{j+1} + a_{j+2}). \quad (30)$$

We can see that  $\psi_j = a_j |\chi_-\rangle$ . It is straightforward to find two normalizable solutions for  $a_j$ 's, which we will denote as  $a_j = \alpha_j$  ( $j = 1, 2, 3, \dots$ ) and  $a_j = \beta_j$  ( $j = 1, 2, 3, \dots$ ). The explicit expressions of  $\alpha_j$  and  $\beta_j$  are

$$\alpha_j = C_\alpha \frac{(-1)^{j+1}}{2^{j-1}}, \quad (31)$$

and

$$\beta_j = C_\beta \frac{(-1)^j(j-1)}{2^{j-2}}, \quad (32)$$

where  $C_\alpha$  and  $C_\beta$  are two normalization constants such that  $\sum_j |\alpha_j|^2 = 1$  and  $\sum_j |\beta_j|^2 = 1$ . It is straightforward to find that  $C_\alpha = \sqrt{3}/2$  and  $C_\beta = \sqrt{27}/80$ .

We can check that the two wave functions  $|\Psi_1\rangle = \sum_j \alpha_j |j\rangle \otimes |\chi_-\rangle$  and  $|\Psi_2\rangle = \sum_j \beta_j |j\rangle \otimes |\chi_-\rangle$  are not orthogonal. The orthogonalization can be achieved by the Gram-Schmidt orthogonalization. We have

$$\begin{aligned} |\Psi_1^o\rangle &= |\Psi_1\rangle, \\ |\Psi_2^o\rangle &= \mathcal{N}(|\Psi_2\rangle - |\Psi_1\rangle \langle \Psi_1 | \Psi_2 \rangle), \end{aligned} \quad (33)$$

where  $\mathcal{N} = \sqrt{5}/2$  is a normalization constant and the superscript “o” stands for “orthogonalization”.

So far, we have focused on  $k_x = 0, \lambda = 0$ . In the neighbourhood of  $k_x = 0, \lambda = 0$ , we can expand the Hamiltonian  $H$  to the first order of  $k_x$  and  $\lambda$ , namely,  $H_i(k_x, \lambda) = H_i(0, 0) + \Delta H_i(k_x, \lambda)$  with

$$\begin{aligned} \Delta H_0(k_x, \lambda) &= \begin{pmatrix} 0 & -ik_x \\ ik_x & 0 \end{pmatrix}, \\ \Delta H_1(k_x, \lambda) &= \begin{pmatrix} 0 & \lambda - ik_x \\ -\lambda + ik_x & 0 \end{pmatrix}. \end{aligned} \quad (34)$$

It is readily seen that

$$\begin{aligned} \langle \chi_- | \Delta H_0 | \chi_- \rangle &= -k_x, \quad \langle \chi_- | \Delta H_1 | \chi_- \rangle = -(k_x + i\lambda), \\ \langle \chi_- | \Delta H_1^\dagger | \chi_- \rangle &= -(k_x - i\lambda). \end{aligned} \quad (35)$$

Straightforward calculations lead to

$$\begin{aligned} \langle \Psi_1^o | \Delta H | \Psi_1^o \rangle &= - \left( \sum_{j=1} \alpha_j^2 + 2 \sum_{j=1} \alpha_j \alpha_{j+1} \right) k_x \\ &= -C_\alpha^2 \left( \sum_{j=1} \frac{1}{2^{2j-2}} - 2 \sum_{j=1} \frac{1}{2^{2j-1}} \right) k_x \\ &= 0, \end{aligned}$$

and

$$\begin{aligned} \langle \Psi_2^o | \Delta H | \Psi_2^o \rangle &= -\mathcal{N}^2 \left[ \sum_j [\beta_j - (\sum_l \alpha_l \beta_l) \alpha_j]^2 + 2 \sum_j \right. \\ &\quad \left. [\beta_j - (\sum_l \alpha_l \beta_l) \alpha_j] [\beta_{j+1} - (\sum_l \alpha_l \beta_l) \alpha_{j+1}] \right] k_x \\ &= -\mathcal{N}^2 \left[ (\sum_l \alpha_l \beta_l)^2 \left( \sum_{j=1} \alpha_j^2 + 2 \sum_{j=1} \alpha_j \alpha_{j+1} \right) \right. \\ &\quad \left. + \left( \sum_{j=1} \beta_j^2 + 2 \sum_{j=1} \beta_j \beta_{j+1} \right) - 2(\sum_l \alpha_l \beta_l) \right. \\ &\quad \left. \times \sum_j (\alpha_j \beta_j + \alpha_j \beta_{j+1} + \alpha_{j+1} \beta_j) \right] k_x \\ &= -\mathcal{N}^2 \left[ \left( \sum_{j=1} \beta_j^2 + 2 \sum_{j=1} \beta_j \beta_{j+1} \right) - 2(\sum_l \alpha_l \beta_l) \right. \\ &\quad \left. \times \sum_j (\alpha_j \beta_j + \alpha_j \beta_{j+1} + \alpha_{j+1} \beta_j) \right] k_x \\ &= -\mathcal{N}^2 \left[ C_\beta^2 \sum_{j=1} \frac{1-j}{2^{2j-4}} - 2(\sum_l \alpha_l \beta_l) C_\alpha C_\beta \sum_j \frac{1}{2^{2j-2}} \right] k_x. \end{aligned}$$

Noting the mathematical identities

$$\begin{aligned} \sum_j \alpha_j \beta_j &= C_\alpha C_\beta \sum_j \frac{1-j}{2^{2j-3}}, \\ \sum_j \frac{1}{2^{2j-2}} &= \frac{1}{C_\alpha^2}, \end{aligned} \quad (36)$$

we can see that

$$\begin{aligned} \langle \Psi_2^o | \Delta H | \Psi_2^o \rangle &= -\mathcal{N}^2 \left[ C_\beta^2 \frac{2(\sum_l \alpha_l \beta_l)}{C_\alpha C_\beta} - 2(\sum_l \alpha_l \beta_l) C_\alpha C_\beta \frac{1}{C_\alpha^2} \right] k_x \\ &= 0. \end{aligned} \quad (37)$$

Similarly, we find that

$$\begin{aligned} \langle \Psi_1^o | \Delta H | \Psi_2^o \rangle &= -\mathcal{N} \left[ \sum_j \left( \alpha_j [\beta_{j+1} - (\sum_l \alpha_l \beta_l) \alpha_{j+1}] \right. \right. \\ &\quad \left. \left. + \alpha_{j+1} [\beta_j - (\sum_l \alpha_l \beta_l) \alpha_j] \right) k_x \right. \\ &\quad \left. + \sum_j \left( \alpha_j [\beta_{j+1} - (\sum_l \alpha_l \beta_l) \alpha_{j+1}] \right. \right. \\ &\quad \left. \left. - \alpha_{j+1} [\beta_j - (\sum_l \alpha_l \beta_l) \alpha_j] \right) i\lambda \right] \\ &= -\mathcal{N} \left[ \left( \sum_j [\alpha_j \beta_{j+1} + \alpha_{j+1} \beta_j - 2(\sum_l \alpha_l \beta_l) \alpha_j \alpha_{j+1}] \right) k_x \right. \\ &\quad \left. + \sum_j (\alpha_j \beta_{j+1} - \alpha_{j+1} \beta_j) i\lambda \right] \\ &= -\mathcal{N} \left( C_\alpha C_\beta \sum_j \frac{1}{2^{2j-2}} \right) (k_x + i\lambda) \\ &= -\frac{\mathcal{N} C_\beta}{C_\alpha} (k_x + i\lambda) \\ &= -\frac{3}{4} (k_x + i\lambda), \\ \langle \Psi_2^o | \Delta H | \Psi_1^o \rangle &= \langle \Psi_1^o | \Delta H | \Psi_2^o \rangle^* = -\frac{3}{4} (k_x - i\lambda). \end{aligned}$$

To summarize the above calculations, we have the following low-energy effective Hamiltonian for the edge states near  $k_x = 0, \lambda = 0$ :

$$\begin{aligned} H_{\text{eff}} &= \begin{pmatrix} \langle \Psi_1^o | \Delta H | \Psi_1^o \rangle & \langle \Psi_1^o | \Delta H | \Psi_2^o \rangle \\ \langle \Psi_2^o | \Delta H | \Psi_1^o \rangle & \langle \Psi_2^o | \Delta H | \Psi_2^o \rangle \end{pmatrix} \\ &= -\frac{3}{4} \begin{pmatrix} 0 & k_x + i\lambda \\ k_x - i\lambda & 0 \end{pmatrix}, \end{aligned} \quad (38)$$

or more compactly,

$$H_{\text{eff}} = \frac{3}{4} (-k_x \sigma_x + \lambda \sigma_y). \quad (39)$$

### Sample occupying $y < 0$

Now we study the sample occupying the  $y < 0$  region (Fig.6(b)), then the edge modes can be obtained by solving the following eigenvalue problem,

$$\begin{pmatrix} H_0 & H_1^\dagger & H_2^\dagger & 0 & 0 & 0 & \cdots \\ H_1 & H_0 & H_1^\dagger & H_2^\dagger & 0 & 0 & \cdots \\ H_2 & H_1 & H_0 & H_1^\dagger & H_2^\dagger & 0 & \cdots \\ 0 & H_2 & H_1 & H_0 & H_1^\dagger & H_2^\dagger & \cdots \\ \vdots & \vdots & \vdots & \vdots & \vdots & \vdots & \ddots \end{pmatrix} \begin{pmatrix} \psi_{-1} \\ \psi_{-2} \\ \psi_{-3} \\ \psi_{-4} \\ \vdots \end{pmatrix} = E \begin{pmatrix} \psi_{-1} \\ \psi_{-2} \\ \psi_{-3} \\ \psi_{-4} \\ \vdots \end{pmatrix} \quad (40)$$

Following the same procedures in the previous section, we first find the solutions for  $k_x = 0$  and  $\lambda = 0$ . We find two wave functions with  $E = 0$ , one of which is  $|\Psi'_1\rangle = \sum_j \alpha_j |j\rangle \otimes |\chi_+\rangle$ , and the other is  $|\Psi'_2\rangle = \sum_j \beta_j |j\rangle \otimes |\chi_+\rangle$ . The orthogonalization of the two wavefunctions are achieved by the Gram-Schmidt orthogonalization,

$$|\Psi'^0\rangle = |\Psi'_1\rangle, \\ |\Psi'^0_2\rangle = \mathcal{N}(|\Psi'_2\rangle - |\Psi'_1\rangle \langle \Psi'_1 | \Psi'_2 \rangle). \quad (41)$$

It is readily checked that

$$\begin{aligned} \langle \chi_+ | \Delta H_0 | \chi_+ \rangle &= k_x, \quad \langle \chi_+ | \Delta H_1 | \chi_+ \rangle = k_x + i\lambda, \\ \langle \chi_+ | \Delta H_1^\dagger | \chi_+ \rangle &= k_x - i\lambda. \end{aligned} \quad (42)$$

Straightforward calculations yield

$$\begin{pmatrix} \langle \Psi'_1^0 | \Delta H | \Psi'_1^0 \rangle & \langle \Psi'_1^0 | \Delta H | \Psi'_2^0 \rangle \\ \langle \Psi'_2^0 | \Delta H | \Psi'_1^0 \rangle & \langle \Psi'_2^0 | \Delta H | \Psi'_2^0 \rangle \end{pmatrix} = \frac{3}{4} \begin{pmatrix} 0 & k_x - i\lambda \\ k_x + i\lambda & 0 \end{pmatrix} \quad (43)$$

thus, the low-energy effective Hamiltonian for the edge state reads

$$H_{\text{eff}} = \frac{3}{4} (k_x \sigma_x + \lambda \sigma_y). \quad (44)$$

### Sample occupying $x > 0$

For sample occupying the  $x > 0$  region (Fig.6(c)), the edge modes can be obtained by solving the following eigenvalue problem,

$$\begin{pmatrix} \tilde{H}_0 & \tilde{H}_1 & \tilde{H}_2 & 0 & 0 & 0 & \cdots \\ \tilde{H}_1^\dagger & \tilde{H}_0 & \tilde{H}_1 & \tilde{H}_2 & 0 & 0 & \cdots \\ \tilde{H}_2^\dagger & \tilde{H}_1^\dagger & \tilde{H}_0 & \tilde{H}_1 & \tilde{H}_2 & 0 & \cdots \\ 0 & \tilde{H}_2^\dagger & \tilde{H}_1^\dagger & \tilde{H}_0 & \tilde{H}_1 & \tilde{H}_2 & \cdots \\ \vdots & \vdots & \vdots & \vdots & \vdots & \vdots & \ddots \end{pmatrix} \begin{pmatrix} \tilde{\psi}_1 \\ \tilde{\psi}_2 \\ \tilde{\psi}_3 \\ \tilde{\psi}_4 \\ \vdots \end{pmatrix} = E \begin{pmatrix} \tilde{\psi}_1 \\ \tilde{\psi}_2 \\ \tilde{\psi}_3 \\ \tilde{\psi}_4 \\ \vdots \end{pmatrix}, \quad (45)$$

where

$$\begin{aligned} \tilde{H}_0(k_y, \lambda) &= \begin{pmatrix} -\frac{13}{4} - \cos 2k_y + 3(\cos k_y + \cos \lambda) - 2 \cos k_y \cos \lambda & 2i \sin k_y \sin \lambda + (\sin 2k_y + 2 \sin k_y \cos \lambda - 3 \sin k_y) \\ -2i \sin k_y \sin \lambda + (\sin 2k_y + 2 \sin k_y \cos \lambda - 3 \sin k_y) & \frac{13}{4} + \cos 2k_y - 3(\cos k_y + \cos \lambda) + 2 \cos k_y \cos \lambda \end{pmatrix}, \\ \tilde{H}_1(k_y, \lambda) &= \begin{pmatrix} \frac{3}{2} - \cos k_y - \cos \lambda & -i \sin \lambda + \sin k_y - (\cos k_y + \cos \lambda - \frac{3}{2}) \\ -i \sin \lambda + \sin k_y + (\cos k_y + \cos \lambda - \frac{3}{2}) & -\frac{3}{2} + \cos k_y + \cos \lambda \end{pmatrix}, \\ \tilde{H}_2(k_y, \lambda) &= \begin{pmatrix} -\frac{1}{2} & -\frac{1}{2} \\ \frac{1}{2} & \frac{1}{2} \end{pmatrix}. \end{aligned} \quad (46)$$

When  $k_y = 0$  and  $\lambda = 0$ ,

$$\tilde{H}_0 = \begin{pmatrix} -\frac{1}{4} & 0 \\ 0 & \frac{1}{4} \end{pmatrix}, \quad \tilde{H}_1 = \tilde{H}_2 = \begin{pmatrix} -\frac{1}{2} & -\frac{1}{2} \\ \frac{1}{2} & \frac{1}{2} \end{pmatrix}. \quad (47)$$

It is not difficult to see that

$$\begin{aligned} \tilde{H}_1 |\xi_+\rangle &= 0, \quad \tilde{H}_1^\dagger |\xi_+\rangle = -\xi_-, \\ \tilde{H}_1 |\xi_-\rangle &= -|\xi_+\rangle, \quad \tilde{H}_1^\dagger |\xi_-\rangle = 0, \\ \tilde{H}_0 |\xi_+\rangle &= -\frac{1}{4} |\xi_-\rangle, \quad \tilde{H}_0 |\xi_-\rangle = -\frac{1}{4} |\xi_+\rangle, \end{aligned} \quad (48)$$

where  $|\xi_\pm\rangle = (1, \pm 1)^T / \sqrt{2}$  are the two eigenvectors of  $\tau_x$ . Following similar procedures as previous sections, we find two solutions at  $E = 0$  for  $k_y = \lambda = 0$ . One is  $|\tilde{\Psi}_1\rangle = \sum_j \alpha_j |j\rangle \otimes |\xi_+\rangle$ , and the other is  $|\tilde{\Psi}_2\rangle = \sum_j \beta_j |j\rangle \otimes |\xi_-\rangle$ . Again

we adopt the Gram-Schmidt orthogonalization to define

$$\begin{aligned} |\tilde{\Psi}_1^0\rangle &= |\tilde{\Psi}_1\rangle, \\ |\tilde{\Psi}_2^0\rangle &= \mathcal{N}(|\tilde{\Psi}_2\rangle - |\tilde{\Psi}_1\rangle \langle \tilde{\Psi}_1 | \tilde{\Psi}_2 \rangle). \end{aligned} \quad (49)$$

In the neighbourhood of  $k_y = 0$  and  $\lambda = 0$ ,  $\tilde{H}_{i=0,1}$  can be expanded to the first order of  $k_y$  and  $\lambda$ :

$$\tilde{H}_i(k_y, \lambda) = \tilde{H}_i(0, 0) + \Delta \tilde{H}_i(k_y, \lambda), \quad (50)$$

with

$$\Delta \tilde{H}_0 = \begin{pmatrix} 0 & k_y \\ k_y & 0 \end{pmatrix}, \quad \Delta \tilde{H}_1 = \begin{pmatrix} 0 & k_y - i\lambda \\ k_y - i\lambda & 0 \end{pmatrix}. \quad (51)$$

It is straightforward to check that

$$\begin{aligned} \langle \xi_+ | \Delta \tilde{H}_0 | \xi_+ \rangle &= k_y, \quad \langle \xi_+ | \Delta \tilde{H}_1 | \xi_+ \rangle = k_y - i\lambda, \\ \langle \xi_+ | \Delta \tilde{H}_1^\dagger | \xi_+ \rangle &= k_y + i\lambda, \end{aligned} \quad (52)$$

which lead to

$$\begin{pmatrix} \langle \tilde{\Psi}_1^o | \Delta H | \tilde{\Psi}_1^o \rangle & \langle \tilde{\Psi}_1^o | \Delta H | \tilde{\Psi}_2^o \rangle \\ \langle \tilde{\Psi}_2^o | \Delta H | \tilde{\Psi}_1^o \rangle & \langle \tilde{\Psi}_2^o | \Delta H | \tilde{\Psi}_2^o \rangle \end{pmatrix} = \frac{3}{4} \begin{pmatrix} 0 & k_x - i\lambda \\ k_x + i\lambda & 0 \end{pmatrix} \quad (53)$$

Therefore, the low-energy effective Hamiltonian for the edge state takes the form of

$$H_{\text{eff}} = \frac{3}{4}(k_y \sigma_x + \lambda \sigma_y). \quad (54)$$

### Sample occupying $x < 0$

Finally, we study the sample occupying the  $x < 0$  region (Fig.6(d)). We need to solve the eigenvalue equation:

$$\begin{pmatrix} \tilde{H}_0 & \tilde{H}_1^\dagger & \tilde{H}_2^\dagger & 0 & 0 & 0 & \cdots \\ \tilde{H}_1 & \tilde{H}_0 & \tilde{H}_1^\dagger & \tilde{H}_2^\dagger & 0 & 0 & \cdots \\ \tilde{H}_2 & \tilde{H}_1 & \tilde{H}_0 & \tilde{H}_1^\dagger & \tilde{H}_2^\dagger & 0 & \cdots \\ 0 & \tilde{H}_2 & \tilde{H}_1 & \tilde{H}_0 & \tilde{H}_1 & \tilde{H}_2^\dagger & \cdots \\ \vdots & \vdots & \vdots & \vdots & \vdots & \vdots & \ddots \end{pmatrix} \begin{pmatrix} \tilde{\psi}_{-1} \\ \tilde{\psi}_{-2} \\ \tilde{\psi}_{-3} \\ \tilde{\psi}_{-4} \\ \vdots \end{pmatrix} = E \begin{pmatrix} \tilde{\psi}_{-1} \\ \tilde{\psi}_{-2} \\ \tilde{\psi}_{-3} \\ \tilde{\psi}_{-4} \\ \vdots \end{pmatrix} \quad (55)$$

Following the same steps as in previous sections, we find two  $E = 0$  modes at  $k_y = 0$  and  $\lambda = 0$ , one of which is  $|\tilde{\Psi}'_1\rangle = \sum_j \alpha_j |j\rangle \otimes |\xi_-\rangle$ , and the other is  $|\tilde{\Psi}'_2\rangle = \sum_j \beta_j |j\rangle \otimes |\xi_-\rangle$ ,

where we continue to use  $|\xi_\pm\rangle = (1, \pm 1)^T / \sqrt{2}$  to denote the two eigenvectors of  $\tau_x$ . After orthogonalization, the wave functions take the form of

$$\begin{aligned} |\tilde{\Psi}'_1^o\rangle &= |\tilde{\Psi}'_1\rangle, \\ |\tilde{\Psi}'_2^o\rangle &= \mathcal{N}(|\tilde{\Psi}'_2\rangle - |\tilde{\Psi}'_1\rangle \langle \tilde{\Psi}'_1 | \tilde{\Psi}'_2 \rangle). \end{aligned} \quad (56)$$

In the neighborhood of  $k_y = \lambda = 0$ , we expand the Hamiltonian to the first order of  $k_y$  and  $\lambda$ :  $\tilde{H}_i(k_y, \lambda) = \tilde{H}_i(0, 0) + \Delta \tilde{H}_i(k_y, \lambda)$ , which satisfy

$$\begin{aligned} \langle \xi_- | \Delta \tilde{H}_0 | \xi_- \rangle &= -k_y, \quad \langle \xi_- | \Delta \tilde{H}_1 | \xi_- \rangle = -(k_y - i\lambda), \\ \langle \xi_- | \Delta \tilde{H}_1^\dagger | \xi_- \rangle &= -(k_y + i\lambda), \end{aligned} \quad (57)$$

therefore, we have

$$\begin{pmatrix} \langle \tilde{\Psi}_1^o | \Delta H | \tilde{\Psi}_1^o \rangle & \langle \tilde{\Psi}_1^o | \Delta H | \tilde{\Psi}_2^o \rangle \\ \langle \tilde{\Psi}_2^o | \Delta H | \tilde{\Psi}_1^o \rangle & \langle \tilde{\Psi}_2^o | \Delta H | \tilde{\Psi}_2^o \rangle \end{pmatrix} = -\frac{3}{4} \begin{pmatrix} 0 & k_y + i\lambda \\ k_y - i\lambda & 0 \end{pmatrix} \quad (58)$$

thus the low-energy effective Hamiltonian for the edge state is given by

$$H_{\text{eff}} = \frac{3}{4}(-k_y \sigma_x + \lambda \sigma_y). \quad (59)$$